CASL-U-2013-0201-000

Power uprates
and plant life extension

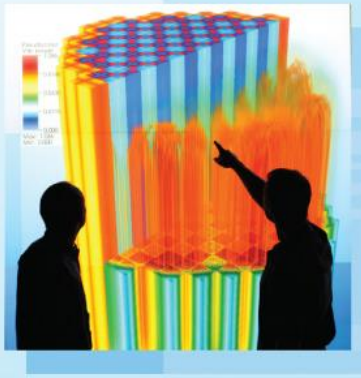

Engineering design
and analysis

Science-enabling
high performance
computing

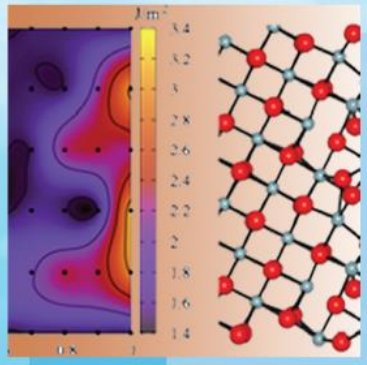

Fundamental science

Plant operational data

Consortium for Advanced Simulation of LWRs

# L3:THM.CFD.P7.07
# Assessment of the Performance of COBRA-TF for the Prediction of Subcooled Boiling Conditions in Rod Bundles

Dr. J. Michael Doster
NCSU

September 30, 2013

U.S. DEPARTMENT OF ENERGY | Nuclear Energy

Final Report

L3.THM.CFD.P7.07

Dr. J. Michael Doster
Nuclear Engineering Department
North Carolina State University

# Assessment of the Performance of COBRA-TF for the Prediction of Subcooled Boiling Conditions in Rod Bundles

September 30, 2013

CASL-U-2013-0201-000

## INTRODUCTION

An assessment has been performed of the performance of COBRA-TF for the prediction of subcooled boiling conditions in heated rod bundles with operating conditions typical of Light Water Reactors. The assessment consists of two parts: 1) A comparison of COBRA-TF predictions to data from three heated bundle experiments and 2) an evaluation of the physics models and constitutive relations incorporated within COBRA-TF. The experiments consisted of a 4 x 4 heated bundle designed primarily to accumulate data for optimization of turbulent mixing coefficients [1] and two 5 x 5 heated bundles designed to simulate subcooled boiling conditions in LWR assemblies [2]. In the 4 x 4 experiment, measured parameters include bundle average exit enthalpy and exit enthalpy and mass flux for the "hot" and "cold" channels. In the 5 x 5 experiments wall temperatures and exit fluid temperatures in the vicinity of the channel exit were available over a wide range of subcooled boiling conditions. COBRA-TF is a 9 field equation model [3], primarily applicable to the simulation of Loss Of Coolant Accidents in Light Water Reactors. COBRA-TF employs conservation equations for three fluid fields, 1) a liquid film, 2) vapor phase and 3) entrained liquid droplets. As a basis of comparison, the experiments were also simulated with the 3 (EN3) and 4 (EN4) equation models in COBRA-EN [4]. The three equation model allows for the calculation of flow quality and void fraction under non equilibrium conditions through the use of user selected empirical correlations. In the four equation model, the liquid phase is allowed to be at non equilibrium conditions and void fraction is computed directly through the vapor mass conservation equation. COBRA-EN has been widely used to simulate the thermal-hydraulic conditions associated with Light Water Reactors under normal operating conditions.

## COMPARISON OF COBRA-TF TO HEATED BUNDLE EXPERIMENTS

### 4 x 4 Rod Bundle Experiment

The rod bundle is symmetric with the channel and rod numberings given in Figure 1.

Table 1: Geometry in inches for the 4x4 bundle.

| Diameter | Pitch | Rod to Wall Spacing | Rod to Rod Spacing | Height |
|---|---|---|---|---|
| 0.422 | 0.555 | 0.148 | 0.133 | 60 |

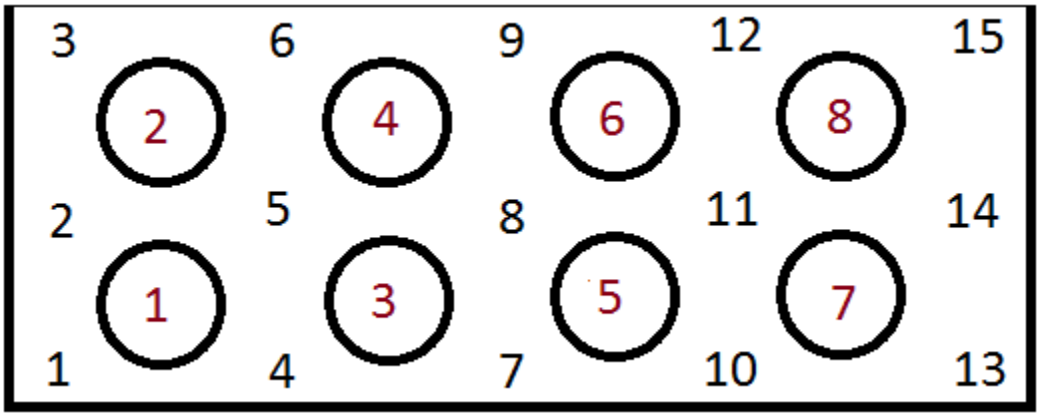


Figure 1: Diagram of the 4x4 bundle.

The conditions for the two cases considered here are shown in Table 2, where the run numbers are consistent with those in the reference [1]. The power was converted to an average heat flux from which the hot and cold rod heat fluxes were obtained. The hot channel heat flux was 108% of the average and the cold channel heat flux was 92% of the average. Rods 1-4 were the hot rods and rods 5-8 were the cold rods. The chosen cases provide a range

of inlet temperatures, along with two distinct flow rates. The operating conditions are similar to nominal operating conditions in Boiling Water Reactors. Measured values include exit enthalpy and mass flux for the hot channel (5) and cold channel (11). The measured and computed values are summarized in Table 3. As seen in Table 3, all the models tested did a reasonable job of predicting the bundle average properties, however significant differences exist for the individual channel exit properties, with COBRA-TF doing a somewhat better job of predicting the channel exit mass flux.

Table 2: Test Case Conditions

| Run Number | Pressure (psia) | Inlet Enthalpy (Btu/lbm) | Average Mass Flux (lbm/hr-ft$^2$) | Assembly Power (MW) |
|---|---|---|---|---|
| 29 | 1200 | 410 | $1 \times 10^6$ | 0.99 |
| 60 | 1200 | 334 | $0.99 \times 10^6$ | 1.5 |

Table 3: Simulated Versus Measured Values for the 4 x 4 Bundle

| | Mass Flux ($10^6$ lbm/hr-ft$^2$) | | | | Enthalpy (Btu/lbm) | | | |
|---|---|---|---|---|---|---|---|---|
| Run 29 | Measured | EN3 | EN4 | TF | Measured | EN3 | EN4 | TF |
| Channel 5 | 0.74 | 0.95 (28%) | 0.95 (28%) | 0.82 (11 %) | 625 | 595 (-4.8%) | 595 (-4.8%) | 590 (-5.6%) |
| Channel 11 | 0.88 | 1.06 (20%) | 1.05 (19 %) | 0.92 (4.5%) | 623 | 570 (-8.5 %) | 570 (-8.5%) | 572 (-8.2)% |
| Bundle Ave | | | | | 563 | 567 (0.7%) | 567 (0.7%) | 561 (-0.4%) |
| | | | | | | | | |
| Run 60 | | | | | | | | |
| Channel 5 | 0.68 | 0.89 (31 %) | 0.91 (34%) | 0.77 (13%) | 635 | 603 (-5.0%) | 602 (-5.1%) | 594 (-6.5 %) |
| Channel 11 | 0.82 | 1.00 (22%) | 1.04 (27%) | 0.90 (9.8%) | 574 | 565 (-1.6%) | 564 (-1.7%) | 567 (1.2%) |
| Bundle Ave | | | | | 550 | 560 (1.8%) | 560 (1.8%) | 550 (0%) |

COBRA-TF and COBRA-EN provide several options for the turbulent mixing models. These options are given in Table 4 below for the mixing models available in COBRA-EN. The mixing models available in COBRA-TF are somewhat more involved and are described below, with the variable definitions available from the COBRA-TF theory manual.

<u>COBRA-TF Mixing Models:</u>

The turbulent exchange of momentum per unit length is defined by:

$$w'^{M}_{ij} = V^{T}_{ij}(G_{iz} - G_{jk})s_k \Delta x$$

Turbulent exchanges of the remaining conserved quantities are calculated by simply replacing the conserved quantity in the equation. Note the turbulent exchange rates are not the same as the turbulent mixing cross flows defined in COBRA-EN.

$$w'^{E}_{ij} = V^{T}_{ij}(\rho_i h_i - \rho_j h_j)s_k \Delta x$$

$$w'^{D}_{ij} = V^{T}_{ij}(\rho_i - \rho_j)s_k \Delta x$$

The transverse velocity is defined as:

$$V^{T}_{ij} = \frac{\beta_{tp}\overline{G}}{\overline{\rho}_{mix}}$$

The differences in the amount of mixing computed in CTF are due to specification of the mixing coefficient, $\beta$.

<u>Default</u>:

$$\beta_{sp} = 0.5\lambda \,\mathrm{Re}^{-0.1}\left[1+\left(\frac{D_{h,jj}}{D_{h,ii}}\right)^{1.5}\right]\left(\frac{D_{h,ii}}{D_{rod}}\right) \quad \text{if } D_{h,ii} < D_{h,jj}$$

$$\beta_{sp} = 0.5\lambda \,\mathrm{Re}^{-0.1}\left[1+\left(\frac{D_{h,ii}}{D_{h,jj}}\right)^{1.5}\right]\left(\frac{D_{h,jj}}{D_{rod}}\right) \quad \text{if } D_{h,jj} < D_{h,ii}$$

$$\lambda = 0.0058\left(\frac{s_k}{D_{rod}}\right)^{-1.46}$$

$$\beta_{tp} = 1 + (\beta_{tp,M} - 1)\left(\frac{x}{x_M}\right) \quad \text{if } x < x_M$$

$$\beta_{tp} = 1 + (\beta_{tp,M} - 1)\left(\frac{x_M - x_0}{x - x_0}\right) \quad \text{if } x > x_M$$

Where,

$$\beta_{tp.M} = \beta_{sp}\Theta_M$$

$$x = \frac{\dot{m}_v}{\dot{m}_v + \dot{m}_l + \dot{m}_e}$$

$$x_M = \frac{\dfrac{0.4[\rho_f(\rho_f - \rho_g)\,\mathrm{g}\,D_h]^{1.2}}{G} + 0.6}{\left(\dfrac{\rho_f}{\rho_g}\right)^{1/2} + 0.6}$$

$$x_0 = 0.75 x_M \, \mathrm{Re}^{0.0417}$$

Note: For the given simulations, $\Theta_M$ was set to 1.0.

Secondary Option:

Instead of allowing CTF to calculate the mixing coefficient via the previous correlation, the user may choose to manually define a two-phase mixing coefficient. For the 4x4 mixture model comparisons, this value was set to the recommended value of 0.05.

Void Drift Cross-flow:

The void drift cross-flow is calculated in a similar manner to the turbulent mixing cross-flow. The cross-flow per unit length of each conserved quantity is given by:

$$w'^{M}_{ij} = -V^{T}_{ij}(G_i + G_j)(\alpha_i - \alpha_j)_{equil} s_k \Delta x$$

$$w'^{E}_{ij} = -V^{T}_{ij}(\alpha_i \rho_i h_i + \alpha_j \rho_j h_j)(\alpha_i - \alpha_j)_{equil} s_k \Delta x$$

$$w'^{D}_{ij} = -V^{T}_{ij}(\alpha_i \rho_i + \alpha_j \rho_j)(\alpha_i - \alpha_j)_{equil} s_k \Delta x$$

Where,

$$(\alpha_i - \alpha_j)_{equil} = \frac{K_a (G_i - G_j)}{\bar{G}}$$

Note: $K_a$ is chosen to be 1.4. In the case of no void drift, this value is set to 0. If Void Drift is present, these values are added to the corresponding turbulent mixing cross flows.

The results in Table 3 were produced with mixing model 1 for COBRA-EN and the default mixing model for COBRA-TF. The corresponding enthalpy and mass flux distributions are illustrated in Figures 2 and 3. Figures 4-7 illustrate the impact of the choice of mixing model on the channel enthalpy and mass flux distributions for the hot and cold channels in Run Number 29. The model coefficients were chosen to insure consistency between the different models tested. As these results indicate, the default mixing model in COBRA-TF consistently out performed the other models, with mixing model 1 giving the best results for COBRA-EN.

Table 4: COBRA-EN Turbulent Mixing Models

| COBRA-EN | Mixing Model | Model Coefficients |
|---|---|---|
| Mixing Model 1 | $w'_k = a(\mathrm{Re})^b \left(\frac{s_k}{l_k}\right) D_k G_k$ | a = 0.0296, b = -0.10 |
| Mixing Model 2 | $w'_k = a(\mathrm{Re})^b D_k G_k$ | a = 0.0071, b = -0.10 |
| Mixing Model 3 | $w'_k = a(\mathrm{Re})^b s_k G_k$ | a = 0.0851, b = -0.10 |
| Mixing Model 4 | $w'_k = a s_k G_k$ | a = 0.02 |

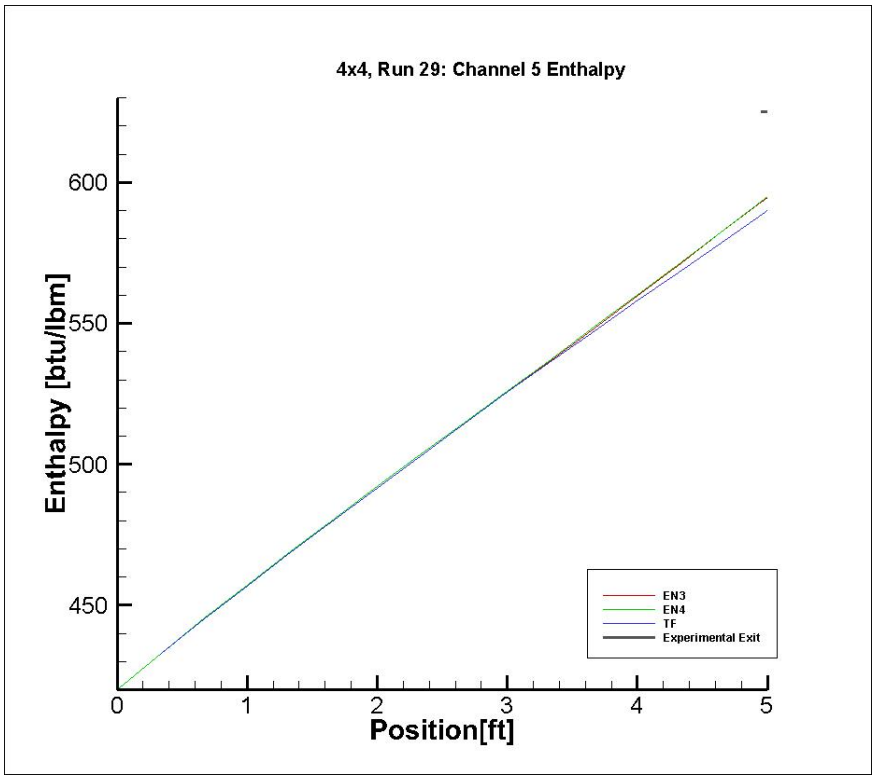


Figure 2: Channel Enthalpy Distributions

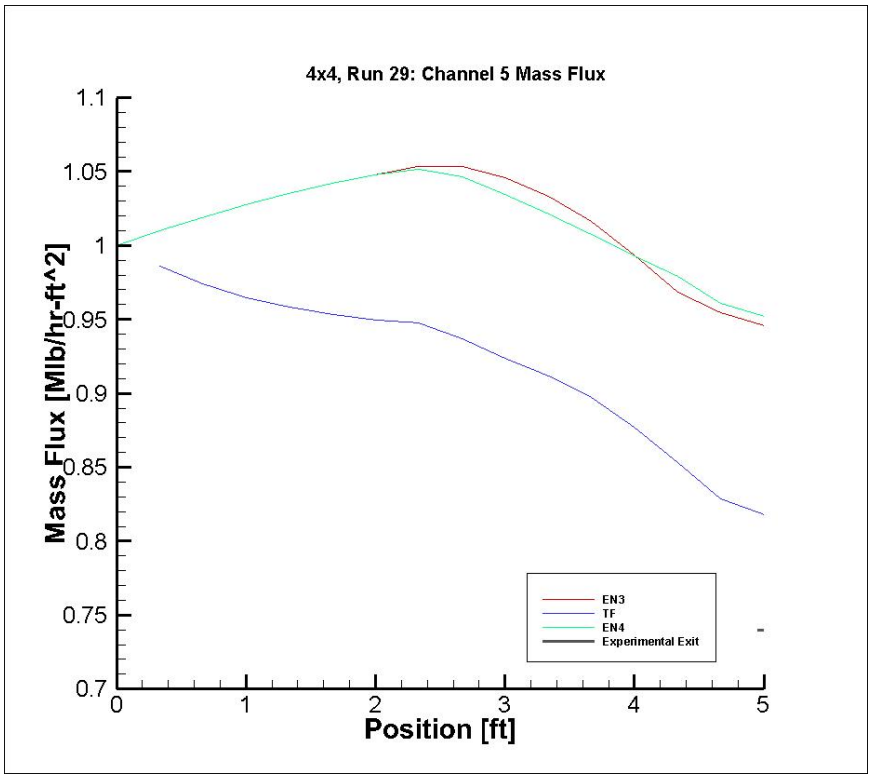


Figure 3: Channel Mass Flux

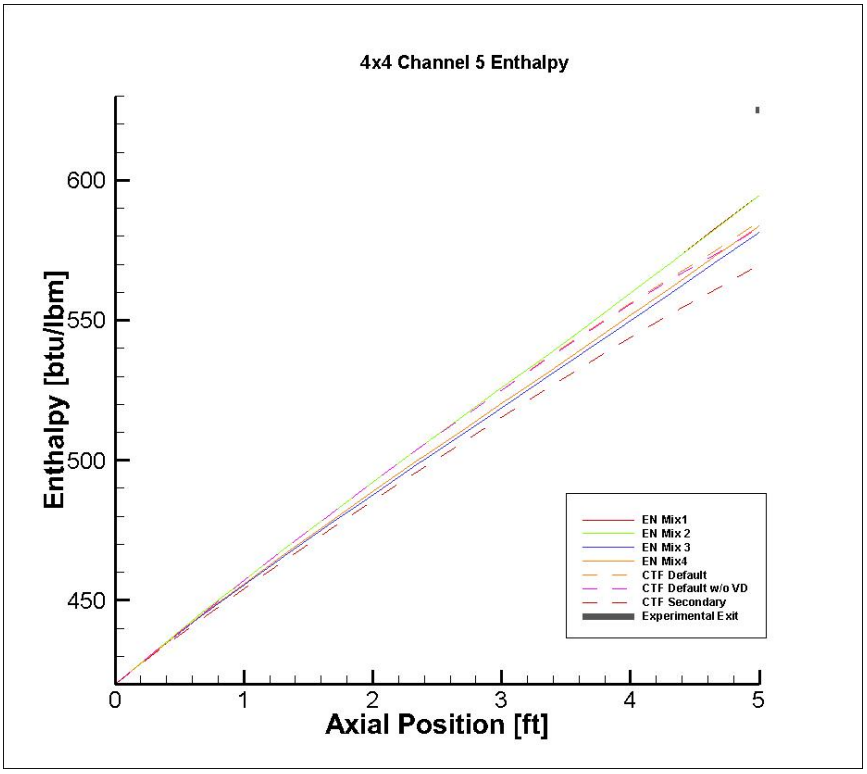


Figure 4: Channel 5 Enthalpy Distribution as a Function of Mixing Model

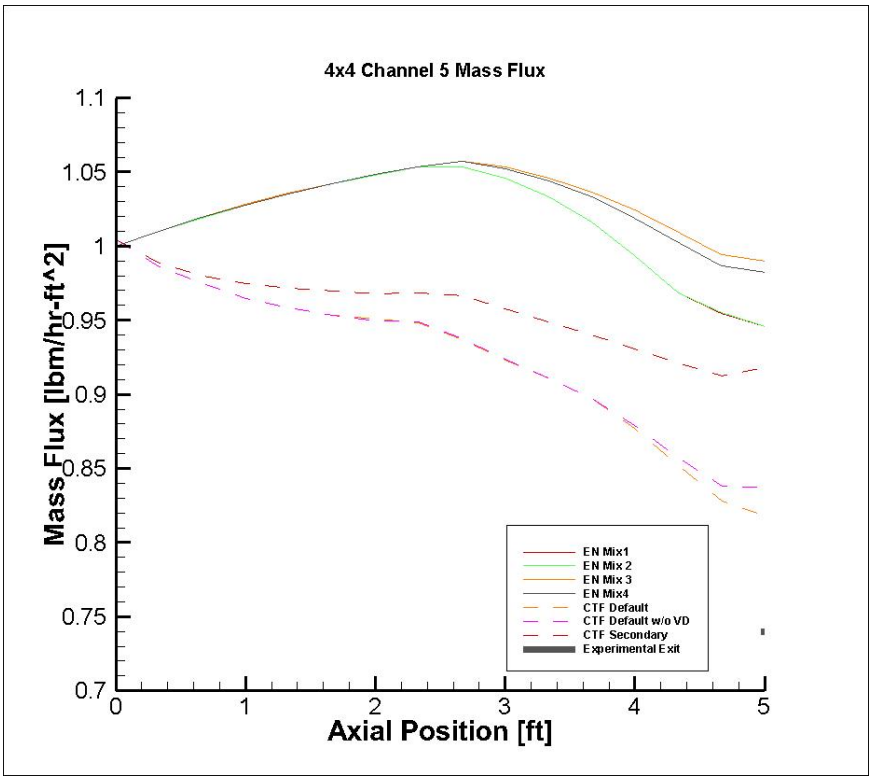


Figure 5: Channel 5 Mass Flux Distribution as a Function of Mixing Model

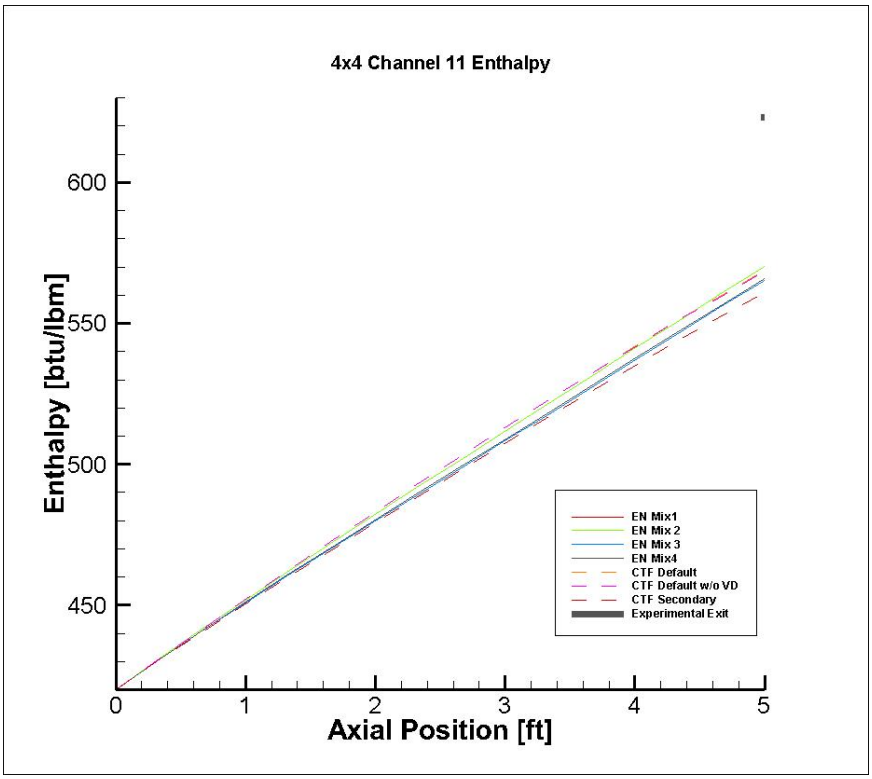


Figure 6: Channel 11 Enthalpy Distribution as a Function of Mixing Model

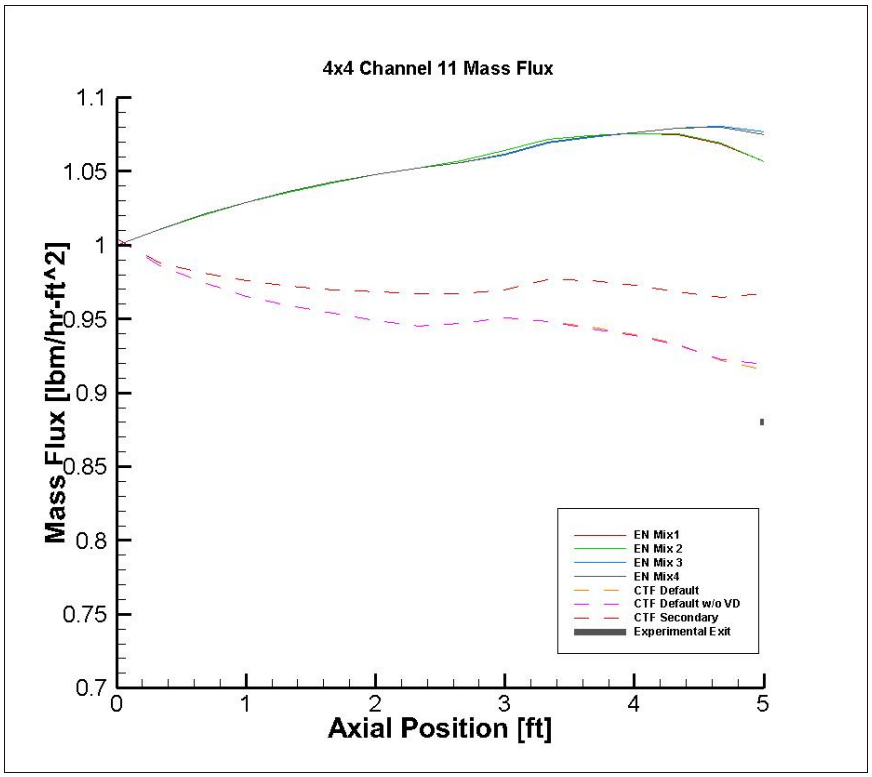


Figure 7: Channel 11 Mass Flux Distribution as a Function of Mixing Model

Of particular interest in this work is the ability of the subchannel methods to predict wall temperatures under subcooled and bulk boiling conditions. The computed wall temperatures are shown in Figure 8 for run number 29. COBRA-TF predicts wall temperatures far greater than those predicted by COBRA-EN. This same behavior was observed in run number 60. In addition to the fluid enthalpy and channel mass flux distributions shown previously, fluid temperature and flow quality distributions are given in Figures 9 and 10. While some differences in the computed values exist, none are significant enough to explain the difference in the wall temperature predictions. Since wall temperature was not a measured parameter in the 4 x 4 experiments, no conclusions could be drawn regarding the relative accuracy of the different model predictions. To address this issue, rod bundle experiments with wall temperature measurement were simulated.

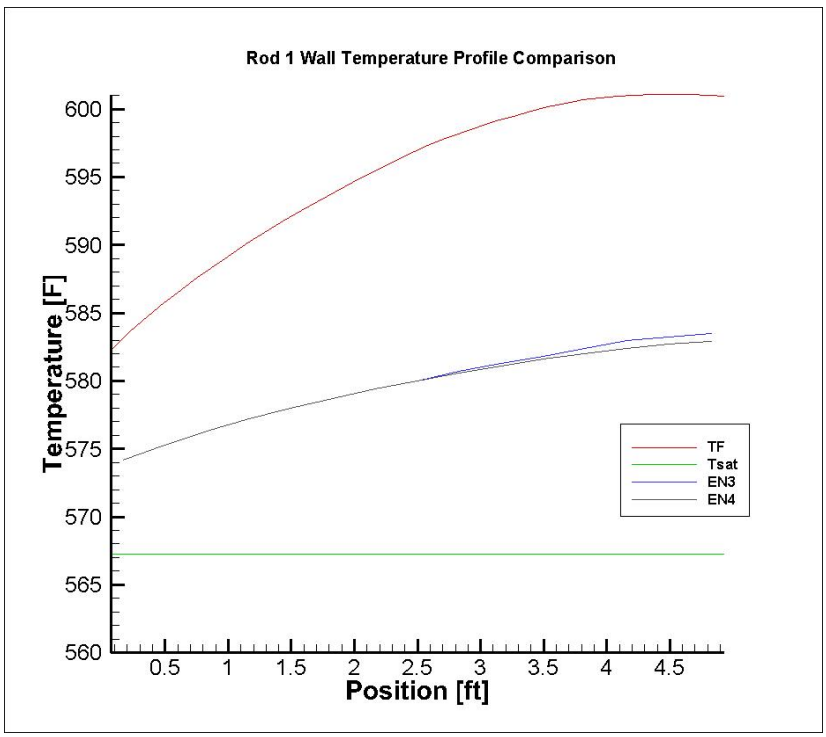


Figure 8: Computed Wall Temperatures for Rod 1 Run # 29

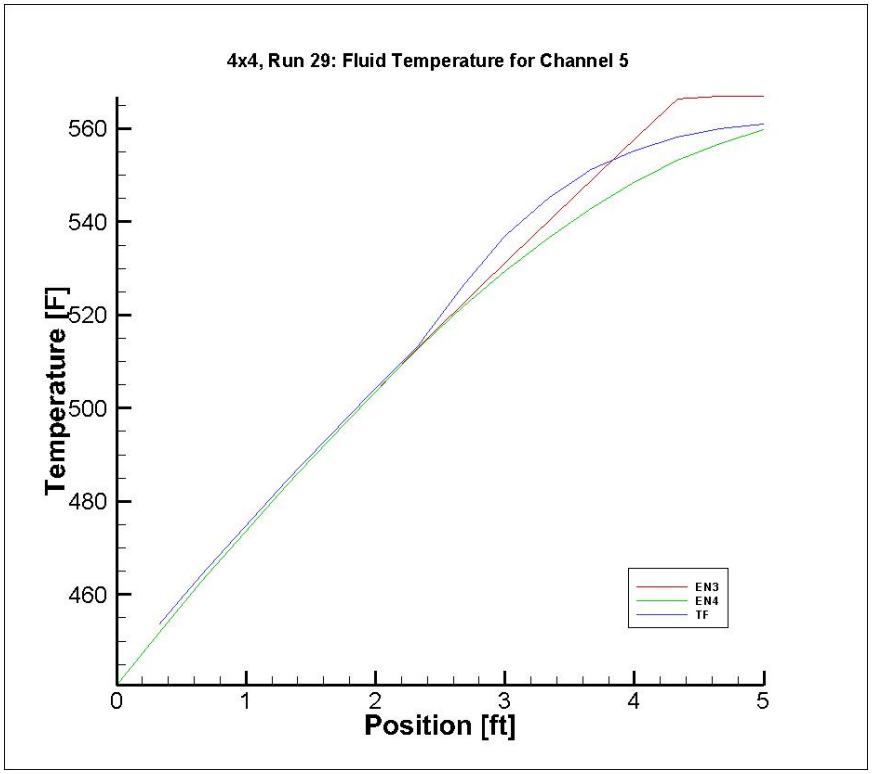


Figure 9: Computed Fluid Temperature Distributions

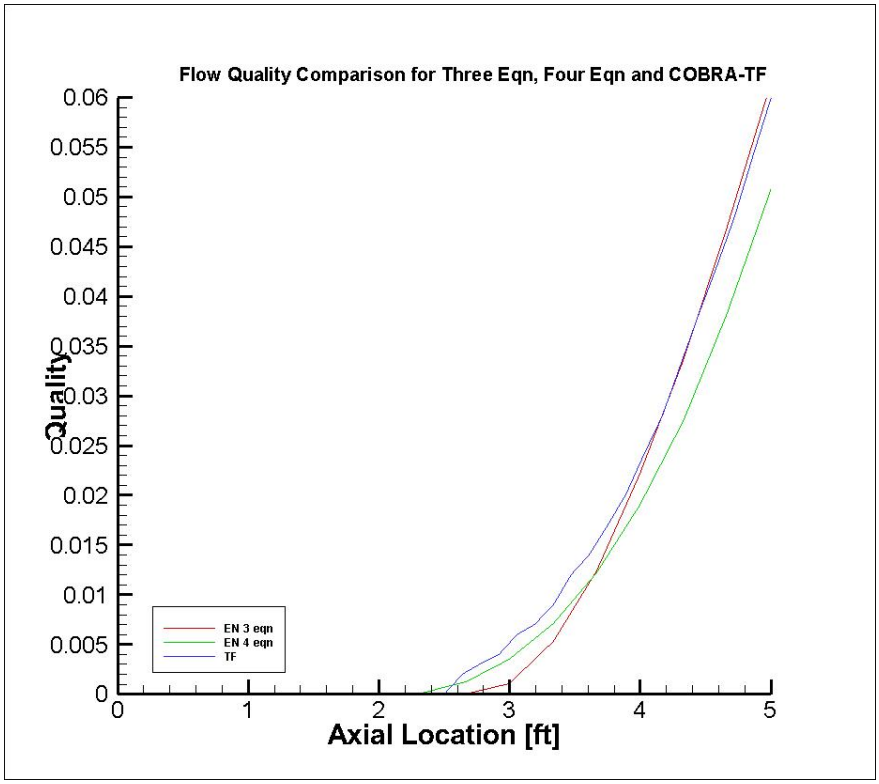


Figure 10: Channel Flow Quality Distributions

**EPRI Rod Bundle Tests**

The EPRI rod bundle experiments provide subcooled boiling data over a wide range of operating conditions typical of nominal PWR operation. Two test bundles have been considered. The bundle dimensions and relative power distributions are provided in Figures 11 and 12. Heat flux is uniform axially. Measurement locations are illustrated in Figure 13. Wall temperatures are measured in the vicinity of the exit grid location. Though not measured, computed flow quality and void distributions are also presented. Simulations have been run with both COBRA-EN and COBRA-TF for test conditions ranging from purely single phase forced convection to subcooled boiling. For some of the test conditions, the 4 Equation model in COBRA-EN failed to converge and only the results from the 3 Equation model are presented. A summary of the test conditions considered for Bundles 74 and 75 are given in Tables 5 and 6. Graphical results are presented for 6 cases: no boiling (Run 50, Bundle 74 and Run 47, Bundle 75), moderate subcooled boiling (Run 55, Bundle 74 and Run 54, Bundle 75) and significant subcooled boiling (Run 57, Bundle 74 and Run 57, Bundle 75). Results from the other cases are similar.

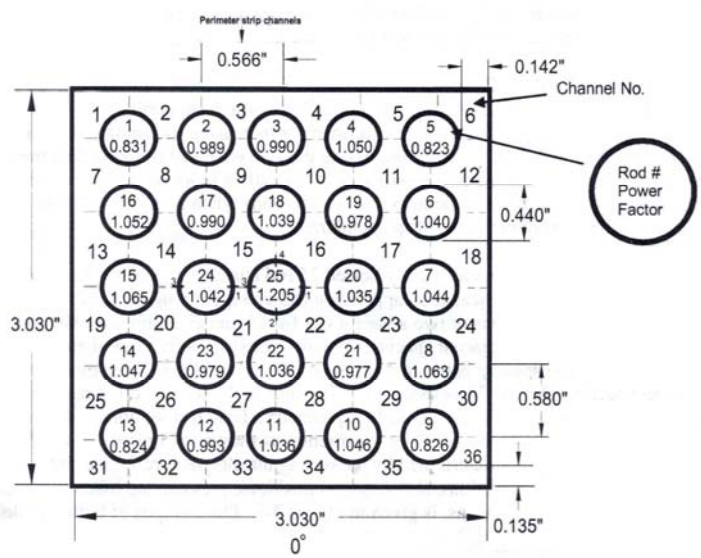


Figure 11: EPRI Test Bundle 74

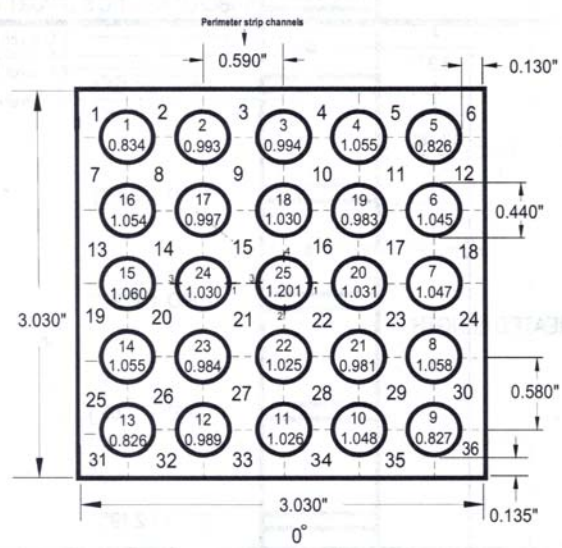


Figure 12: EPRI Test Bundle 75

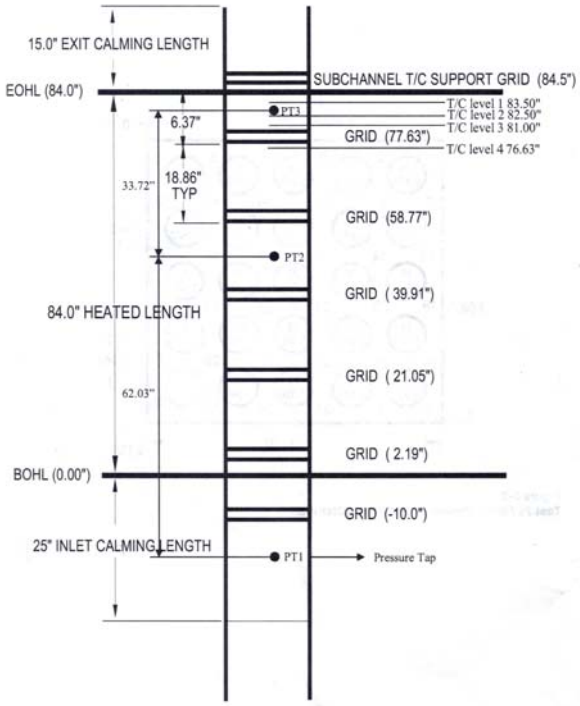


Figure 13: EPRI Test Bundle Axial Geometry

Table 5: Test Case Conditions Bundle 74 (P=2254 psia)

| Run # | $T_{inlet}$ (F) | Exit $x_e$ | Mass Flux ($10^6$ lbm/hr-ft$^2$) | $\overline{q}''$ ($10^5$ Btu/hr-ft$^2$) | $q''_{max}$ ($10^5$ Btu/hr-ft$^2$) |
|---|---|---|---|---|---|
| 11 | 564 | -0.171 | 2.25 | 2.83 | 3.40 |
| 12 | 563 | -0.144 | 2.24 | 3.33 | 4.00 |
| 50 | 563 | -0.223 | 2.26 | 1.98 | 2.38 |
| 55 | 562 | -0.081 | 2.65 | 4.48 | 5.38 |
| 57 | 562 | -0.031 | 2.26 | 5.28 | 6.34 |

Table 6: Test Case Conditions Bundle 75 (P=2249 psia)

| Run # | $T_{inlet}$ (F) | Exit $x_e$ | Mass Flux ($10^6$ lbm/hr-ft$^2$) | $\overline{q}''$ ($10^5$ Btu/hr-ft$^2$) | $q''_{max}$ ($10^5$ Btu/hr-ft$^2$) |
|---|---|---|---|---|---|
| 47 | 564 | -0.210 | 2.25 | 2.17 | 2.61 |
| 51 | 563 | -0.160 | 2.25 | 2.94 | 3.54 |
| 53 | 565 | -0.130 | 2.24 | 3.43 | 4.14 |
| 54 | 564 | -0.080 | 2.25 | 4.49 | 5.41 |
| 56 | 565 | -0.025 | 2.24 | 5.24 | 6.32 |
| 57 | 563 | -0.006 | 2.23 | 5.71 | 6.88 |

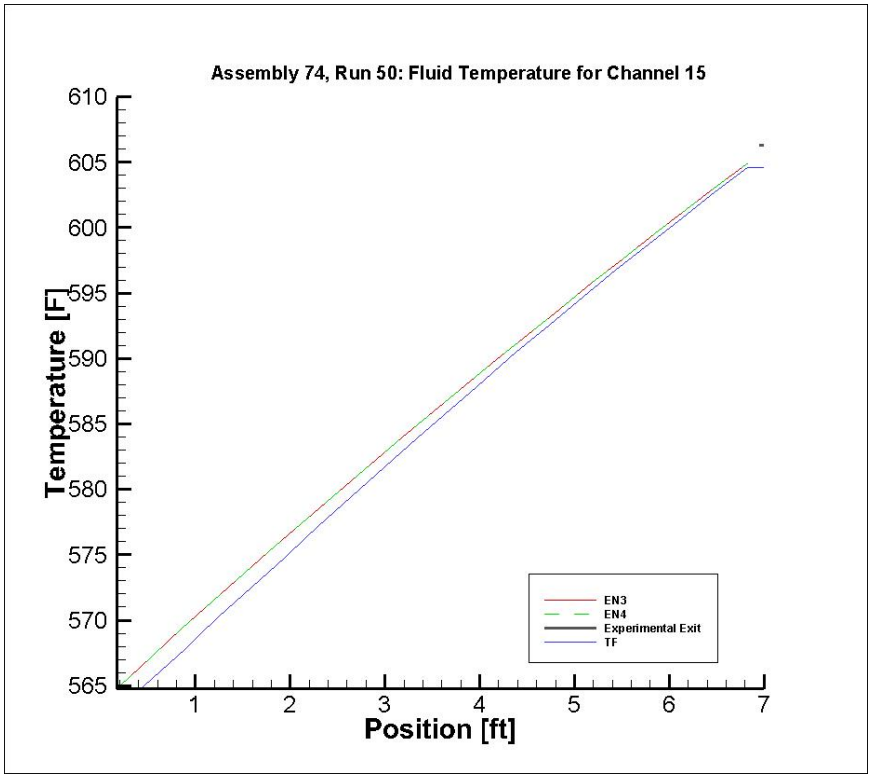


Figure14: Run 50 Bundle 74 Fluid Temperature Distributions

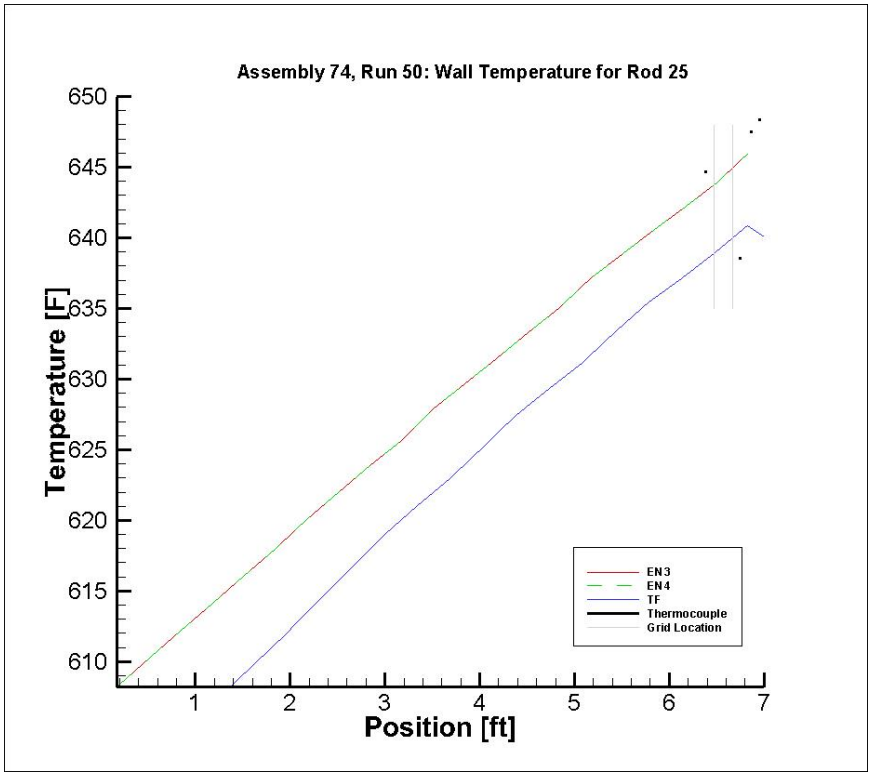


Figure 15: Run 50 Bundle 74 Wall Temperature Distributions

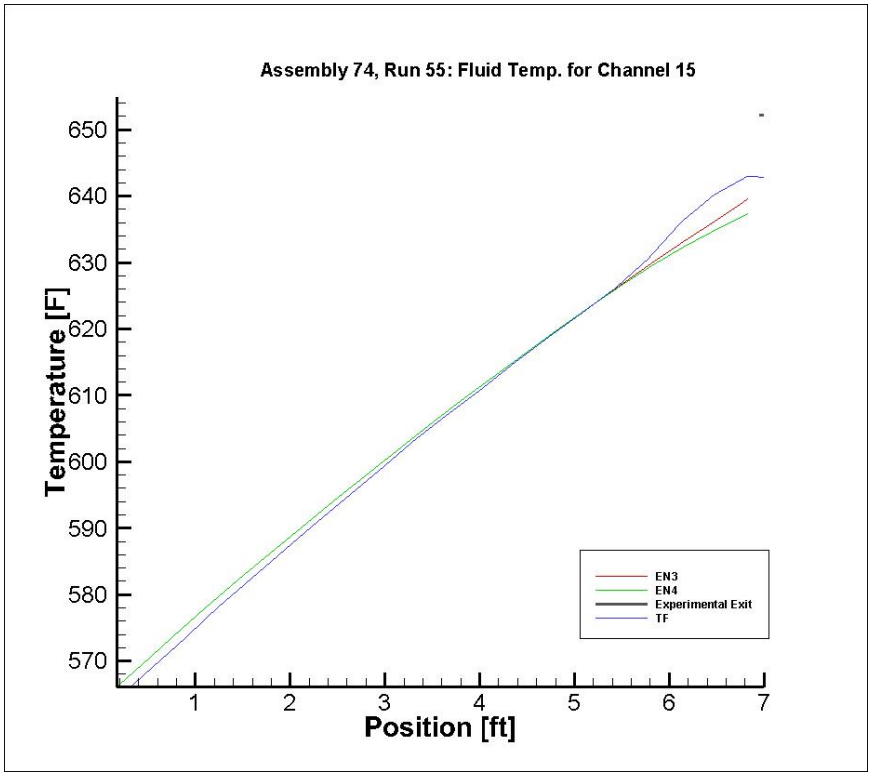


Figure 16: Run 50 Bundle 74 Fluid Temperature Distributions

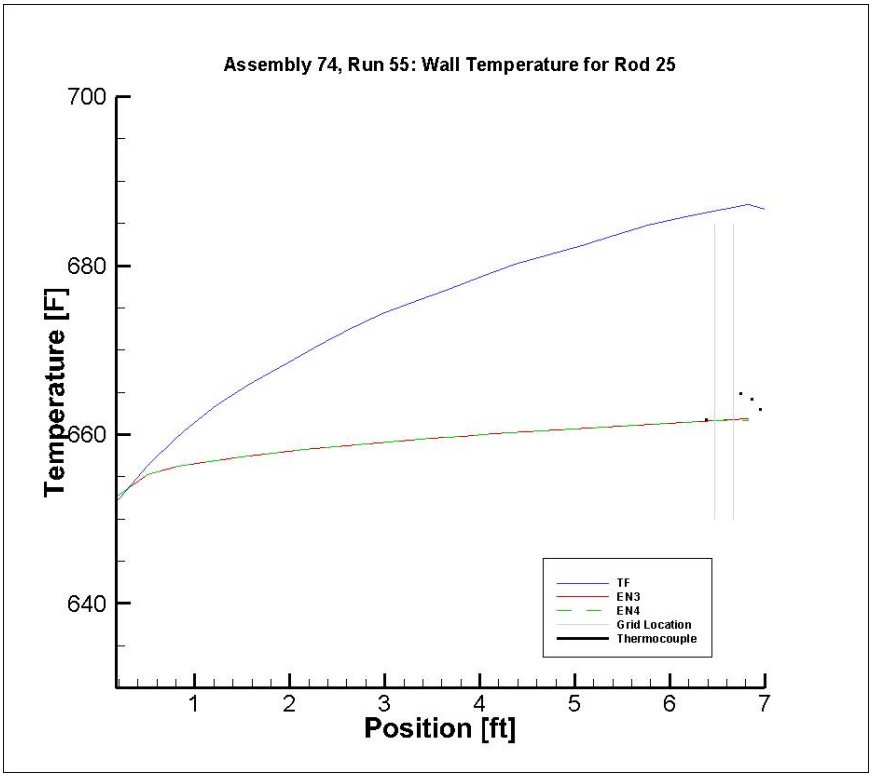


Figure 17: Run 55 Bundle 74 Wall Temperature Distributions

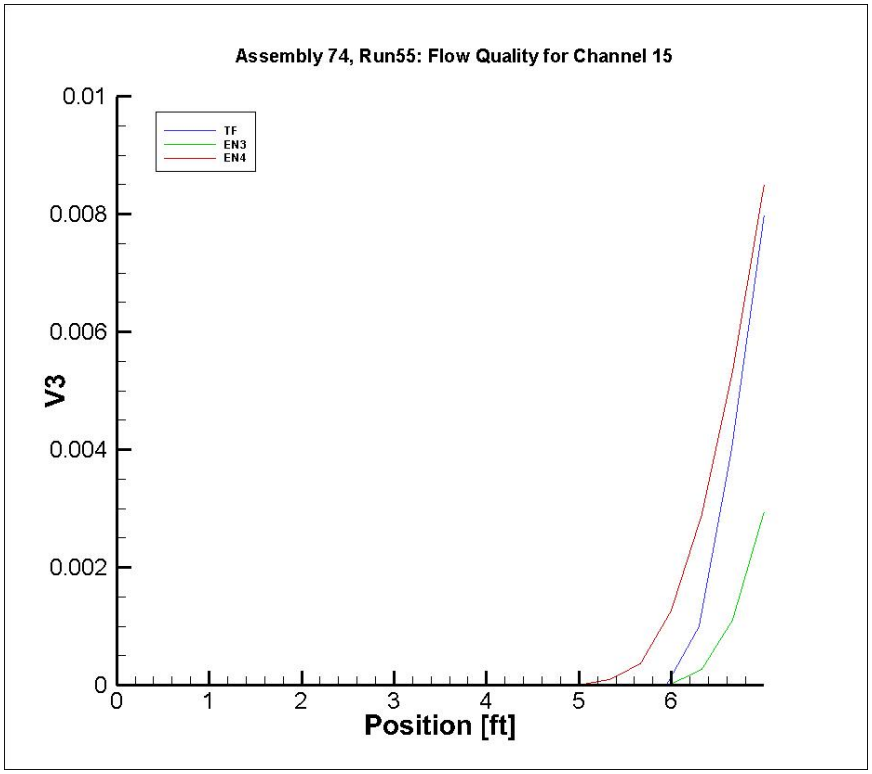


Figure 18: Run 55 Bundle 74 Flow Quality Distributions

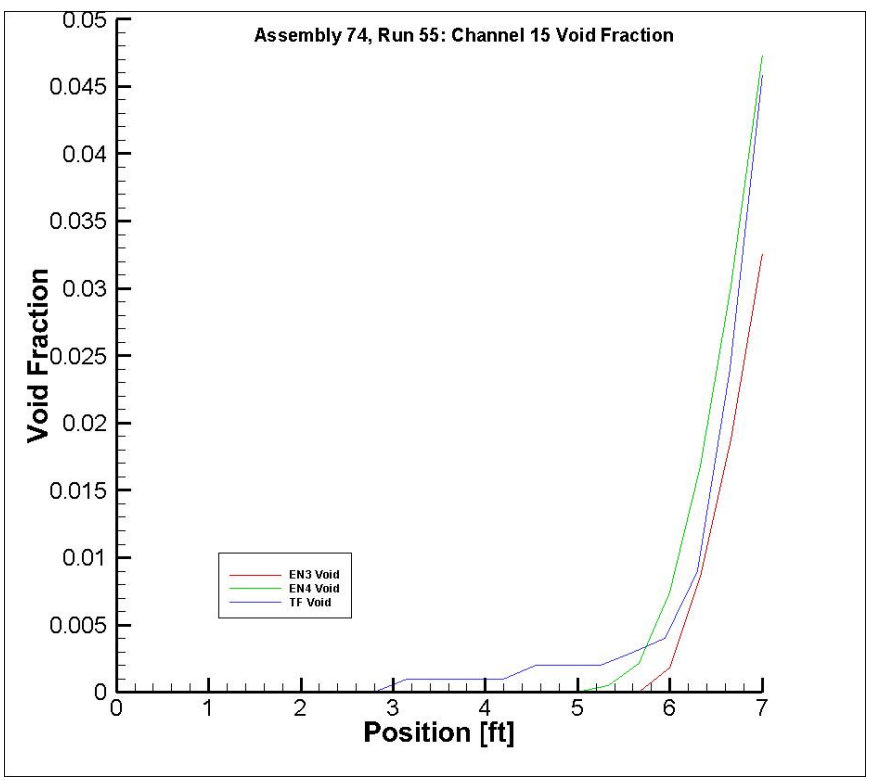


Figure 19: Run 55 Bundle 74 Void Distributions

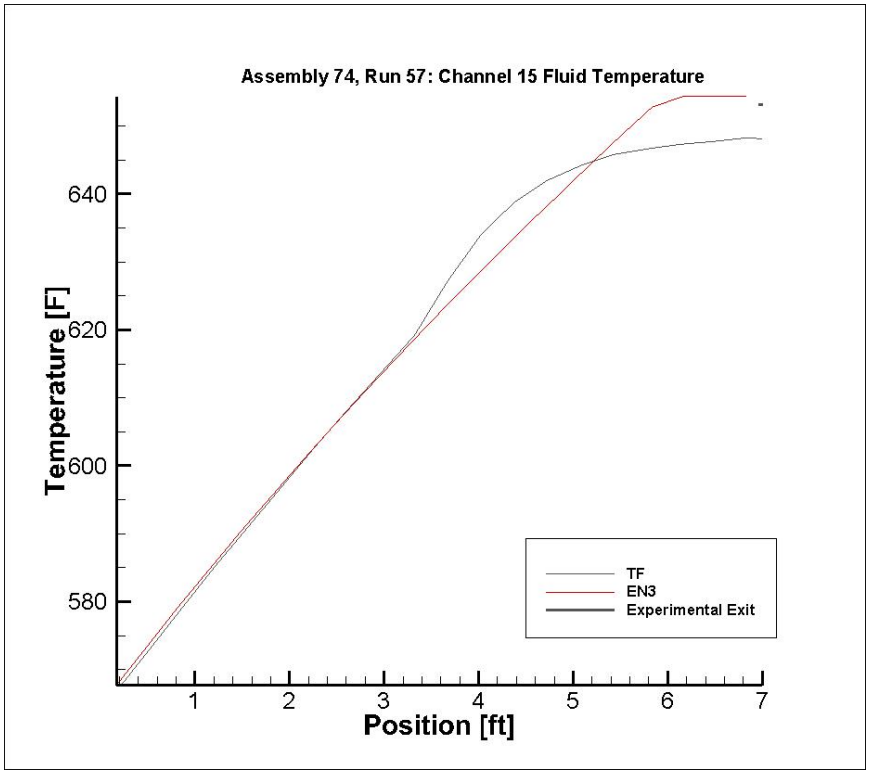


Figure 20: Run 57 Bundle 74 Fluid Temperature Distributions

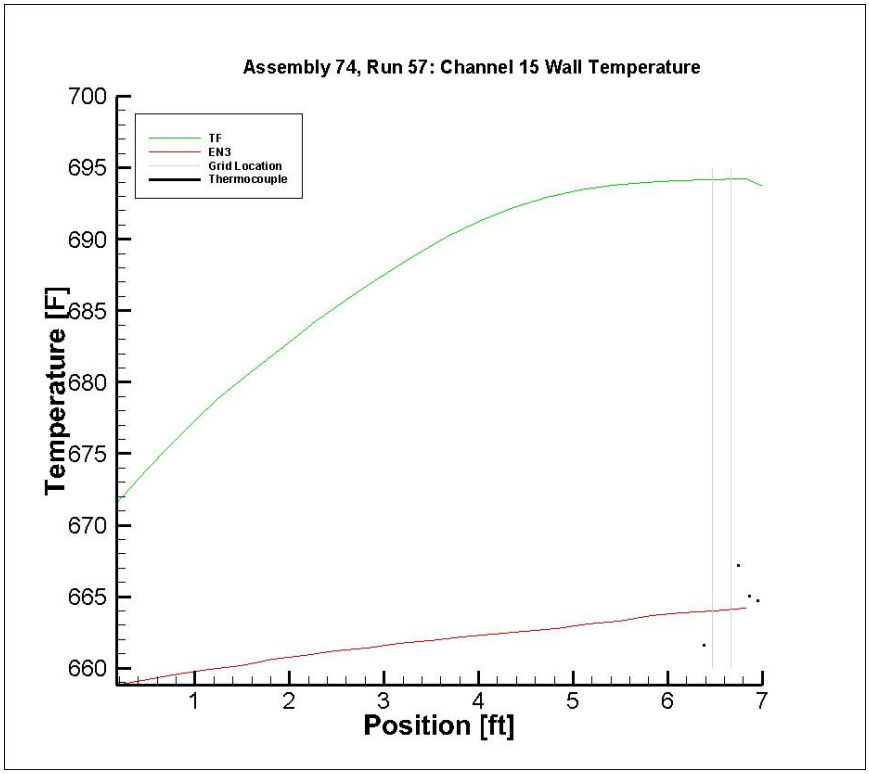


Figure 21: Run 57 Bundle 74 Wall Temperature Distributions

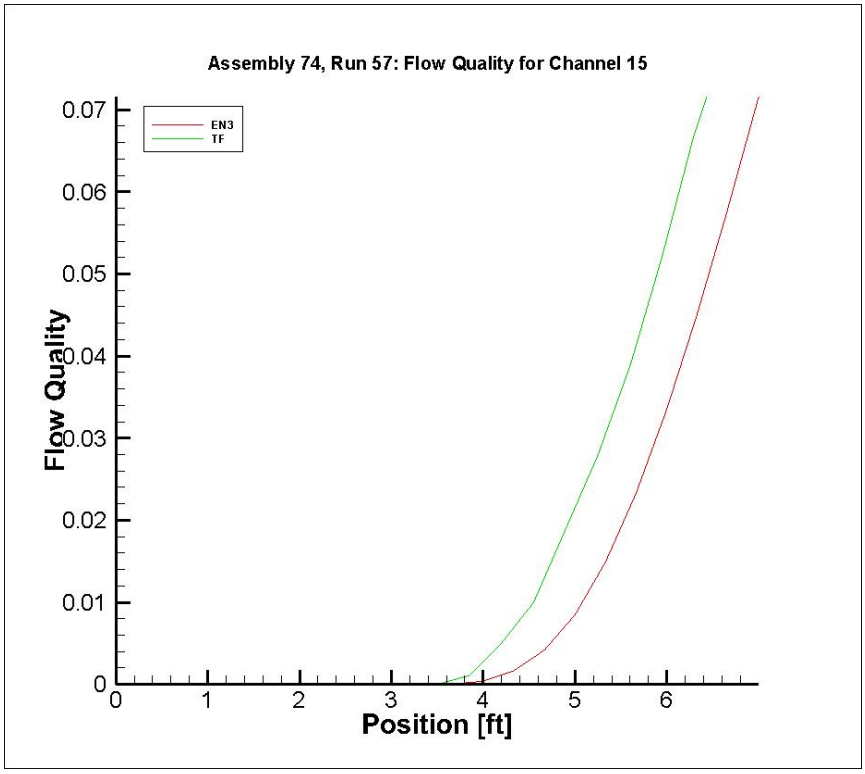


Figure 22: Run 57 Bundle 74 Flow Quality Distributions

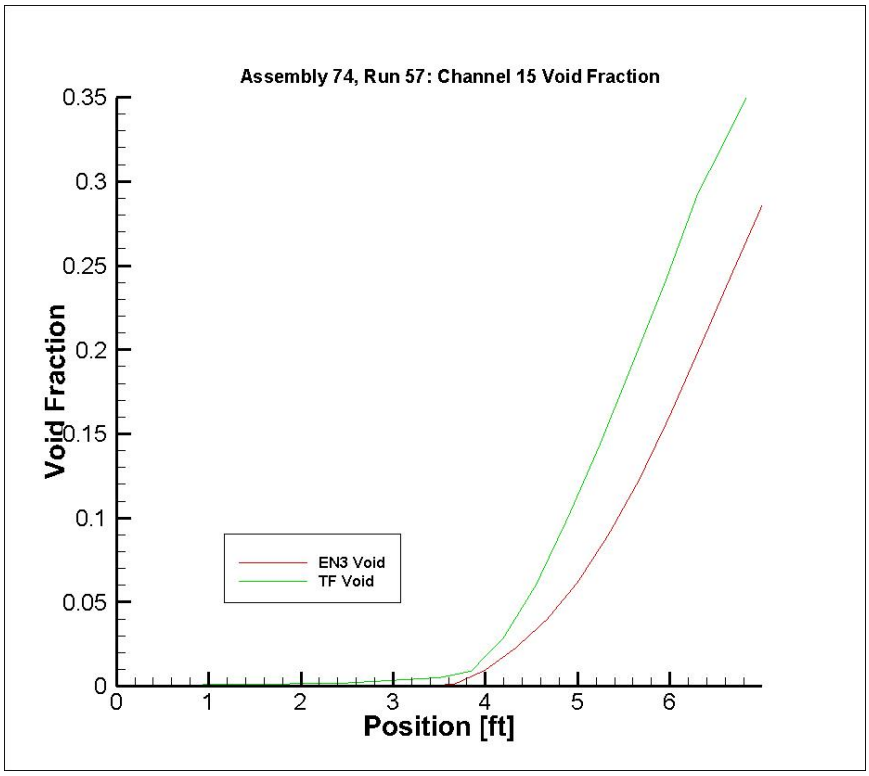


Figure 23: Run 57 Bundle 74 Void Distributions

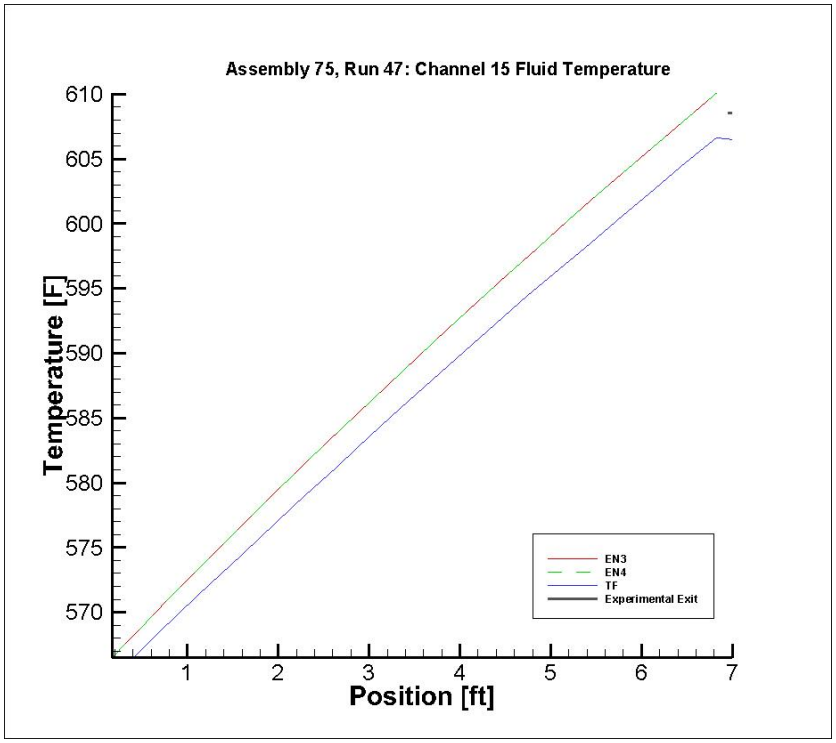


Figure 24: Run 47 Bundle 75 Fluid Temperature Distributions

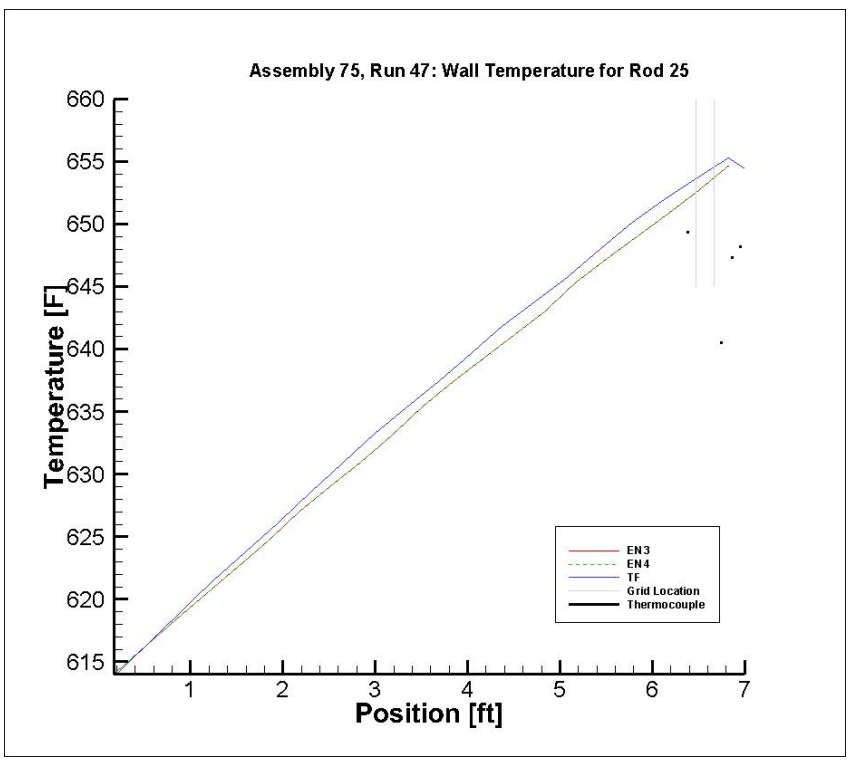


Figure 25: Run 47 Bundle 75 Wall Temperature Distributions

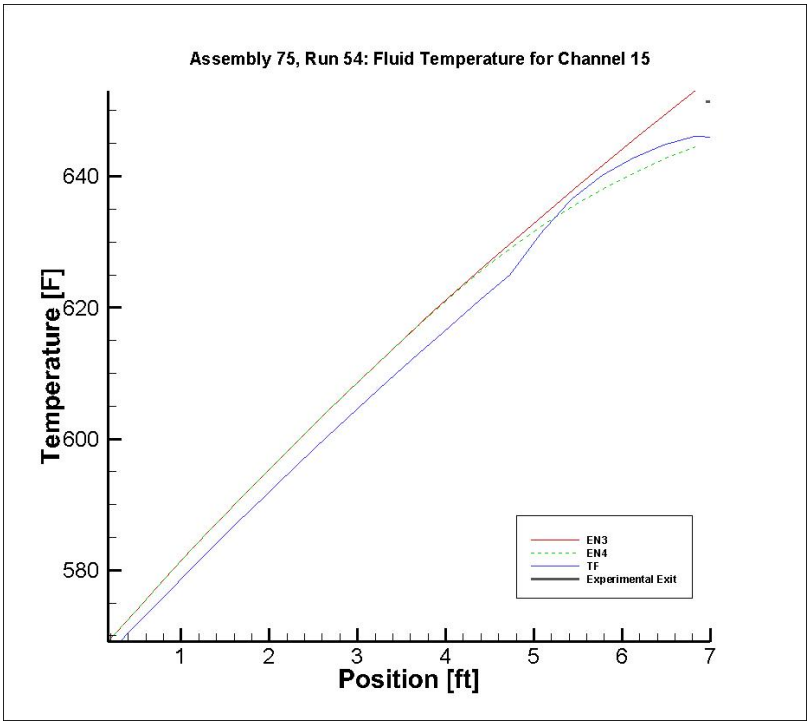


Figure 26: Run 54 Bundle 75 Fluid Temperature Distributions

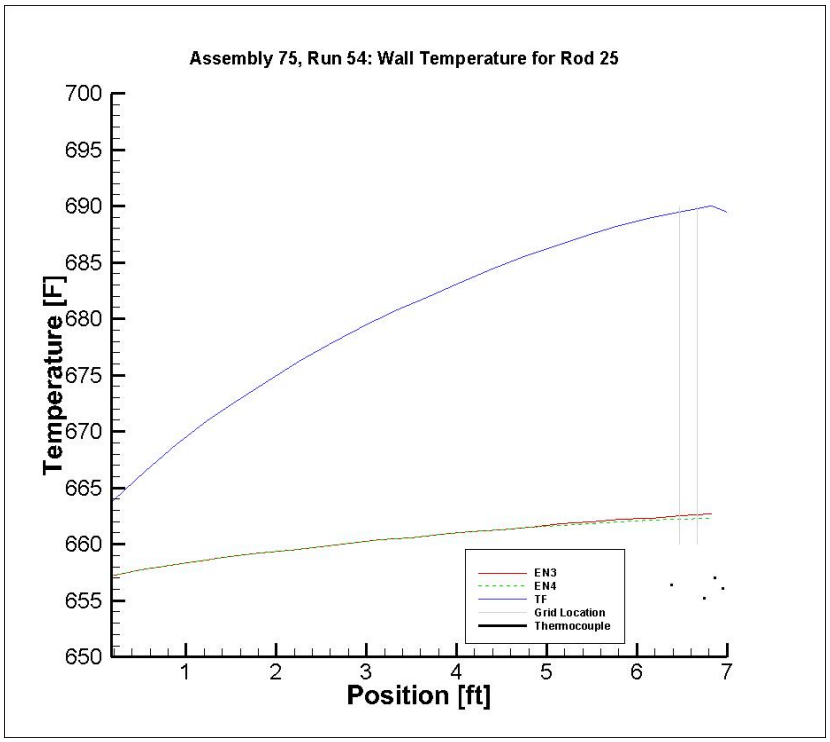


Figure 27: Run 54 Bundle 75 Wall Temperature Distributions

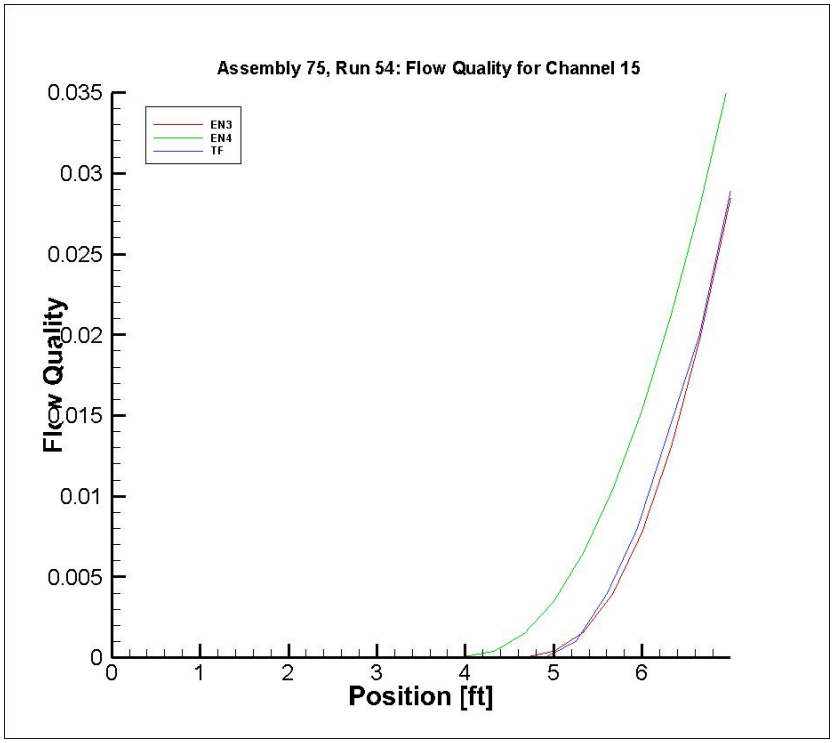


Figure 28: Run 54 Bundle 75 Flow Quality Distributions

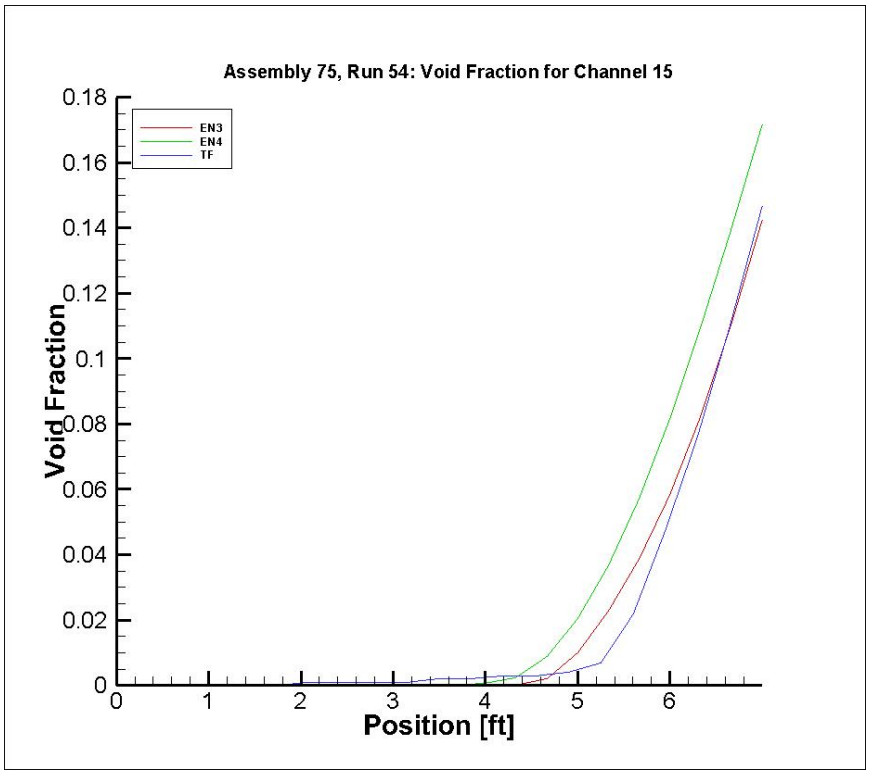


Figure 29: Run 54 Bundle 75 Void Distributions

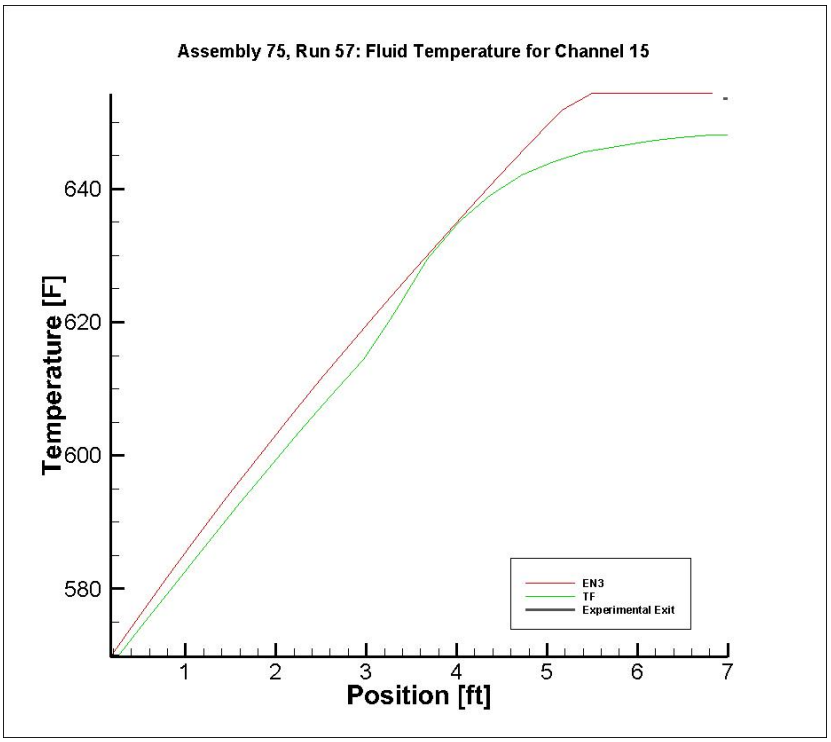


Figure 30: Run 57 Bundle 75 Fluid Temperature Distributions

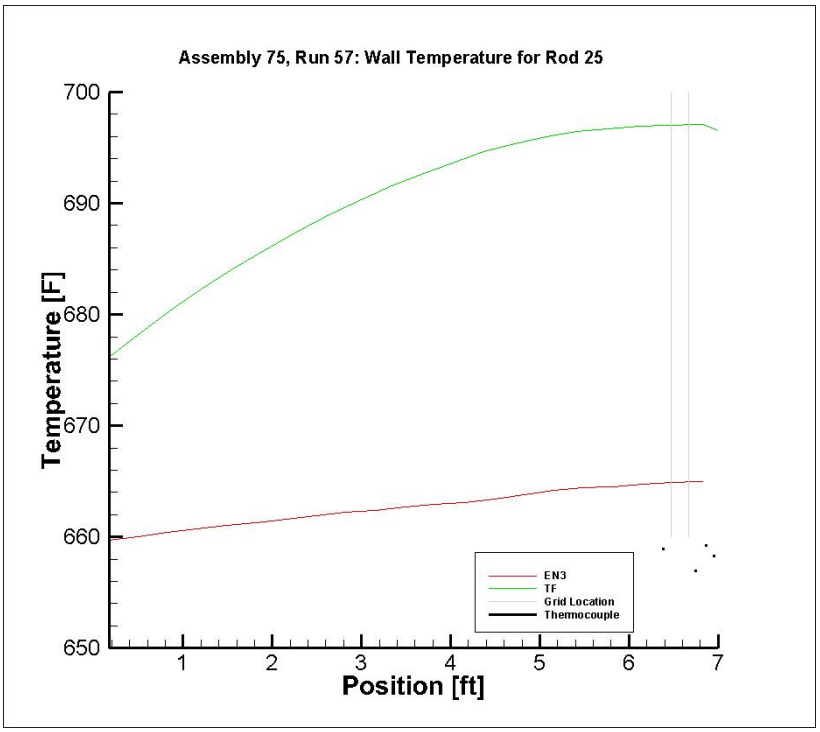


Figure 31: Run 57 Bundle 75 Wall Temperature Distributions

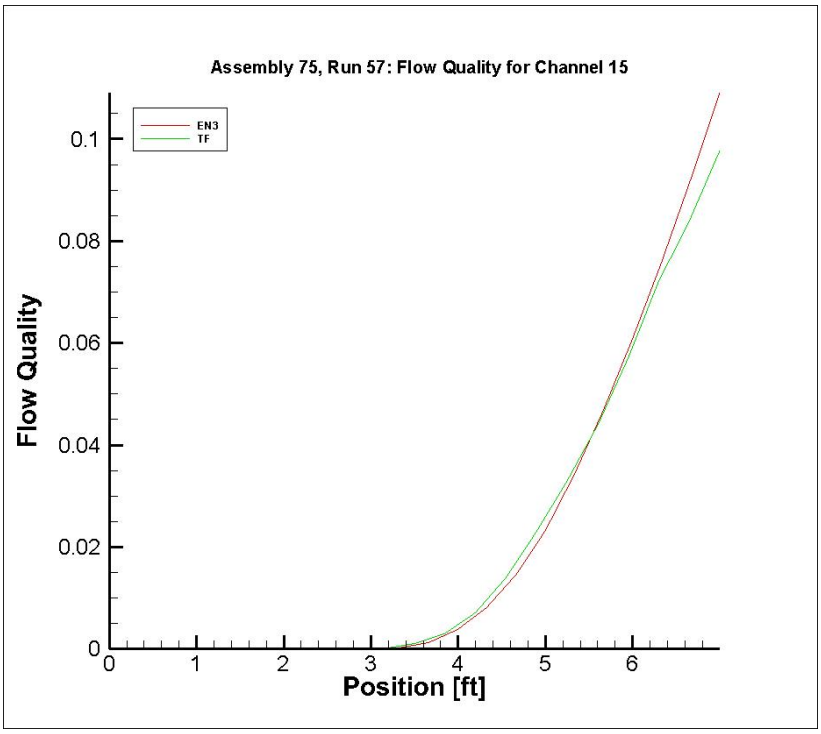


Figure 32: Run 57 Bundle 75 Flow Quality Distributions

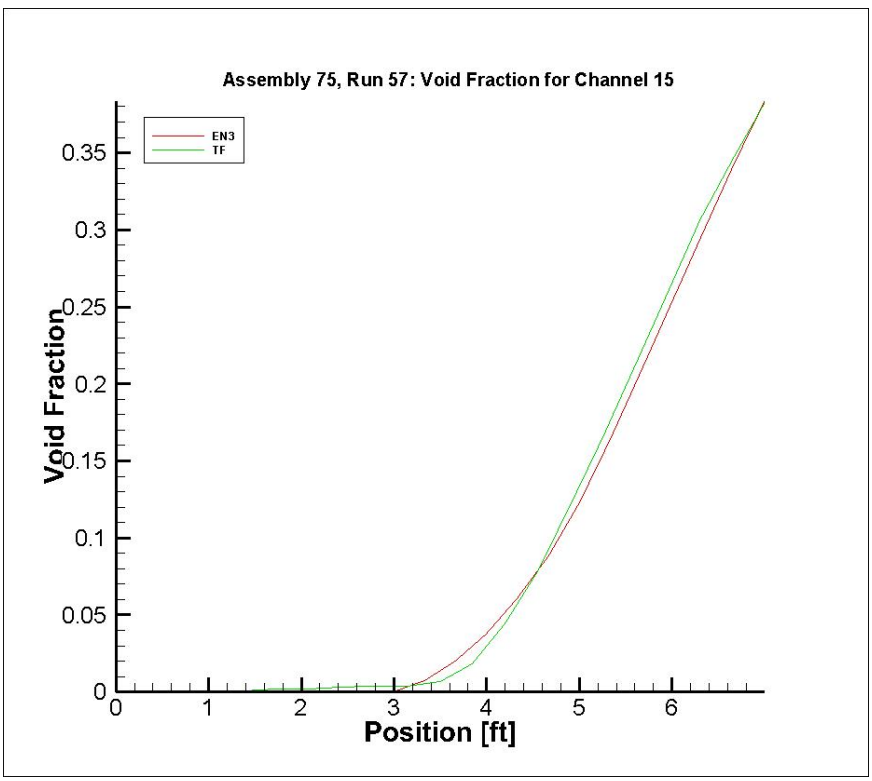


Figure 33: Run 57 Bundle 75 Void Distributions

Fluid Temperature Distributions

In all cases examined, COBRA-EN and COBRA-TF did a reasonable job of predicting channel exit fluid temperatures, and for those cases with no boiling the temperature distributions displayed similar behavior. However, for those cases with boiling, deviations in the liquid phase temperatures were observed. The 4 Equation model in COBRA-EN correctly showed a reduction in liquid phase temperature relative to the 3 Equation model as a result of the non equilibrium conditions associated with subcooled boiling. COBRA-TF displayed an increase in the liquid phase temperature after the onset of subcooled boiling. Investigation into the cause of this increase revealed that COBRA-TF allocates all wall heat transfer to the liquid phase under two phase conditions. While this might be appropriate under annular flow conditions, under subcooled boiling this energy partitioning neglects that component of wall heat transfer which goes directly into the vapor phase. This over predicts the energy content of the liquid phase and over predicts the liquid phase temperature.

Wall Temperature Distributions

For the case of pure single phase forced convection both models predicted similar wall temperature profiles and were in reasonable agreement with the experimental results. However, as with the 4 x 4 bundle results, after the onset of boiling, COBRA-TF predicts significantly higher wall temperatures than COBRA-EN, with the COBRA-EN results much closer to the measured values. This behavior has been observed in all cases examined. Investigation into the differences in the heat transfer models used in the two codes showed that in the nucleate boiling regime, COBRA-EN uses a variant of the Thom correlation, a well known nucleate boiling correlation. COBRA-TF uses the Chen correlation for all two-phase conditions. The Chen correlation was developed for relatively low pressure, high quality conditions associated with Forced Convection Vaporization and is not strictly valid for the high pressure, high heat flux, low quality, subcooled conditions of interest in nominal PWR operations. For annular flow conditions, the Chen correlation would be the more applicable wall heat transfer model but is inappropriate for the conditions simulated here. The change in slope of the wall temperature at the channel exit results from the setting the axial peaking factor to zero at the ends of the rods as recommended in the input processor.

Flow Quality and Void Distributions

The 3 Equation model in COBRA-EN uses a standard profile fit model with an associated bubble departure point correlation to determine the flow quality under non equilibrium conditions. Void fraction can then be determined by a void-quality model. In the 4 Equation COBRA-EN model, void fraction is computed directly from the vapor mass equation and flow quality through the Fundamental Void-Quality-Slip relation where slip ratio is available from a user selected correlation. Void production at the wall is based on an empirically based vapor generation rate correlation. Though COBRA-TF and COBRA-EN predict similar locations within the channel at which the flow quality is greater than zero, COBRA-TF predicts non zero void at significantly lower locations, even when the flow quality is predicted to be zero.

At the onset of a simulation, CTF assumes the presence of all phases. In order for the solution to proceed smoothly, CTF imposes a small non-zero value as a minimum for the vapor void fraction. This allows the fluid to be approximated as single-phase prior to boiling even though the full set of fluid field equations are being solved at each solution step. The vapor void fraction minimum used in CTF is $10^{-6}$. This method is also used in RELAP-5, where the minimum void fraction is set to $10^{-5}$. The calculation of flow quality is simply evaluated from the phasic mass fluxes where the flow quality is defined as

$$x = \frac{G_v}{G_v + G_l}$$

Even though CTF will always predict that void can exist within the channel, flow quality does not begin to develop until a non-zero vapor velocity (either axial or lateral) solution is obtained from the vapor momentum equation. This allows the potential for significant void predictions well before the fluid would be expected to be two-phase.

## COBRA-TF MODELING SUMMARY

In addition to the modeling assumptions which directly affect the simulation of the heated bundle experiments discussed above, the following discussion relates to the ability of COBRA-TF to adequately simulate subcooled boiling conditions of interest to Light Water Reactor operation.

Thermophysical Properties

a) Saturated Liquid and Vapor Properties

Saturated liquid and vapor enthalpies are calculated as a function of pressure based on expressions developed for EPRI's RETRAN-02 code. Other saturated state properties are then interpolated from lookup tables in terms of these enthalpies. The expressions for enthalpy are given in the CTF theory manual along with the look up tables. The CTF manual states that this approach provides values that are in close agreement to the 1968 ASME and 1984 NBS/NRC steam tables.

b) Superheated vapor properties

Superheated vapor properties are provided by expressions developed by Keenan and Keyes, Wagner and Kruse, and ASME . The expressions and references to their source are provided in the CTF theory manual.

c) Subcooled Liquid properties

For all properties other than density, the subcooled liquid properties are taken as the saturated liquid values at the given subcooled liquid enthalpy. This neglects the pressure dependence on subcooled properties. The liquid specific volume is obtained by a functional relationship involving liquid enthalpy and pressure. No reference is given for this relationship, however it is provided in the CTF theory manual.

For consistency, the thermophysical properties in COBRA-TF should be replaced with those used in the other thermal-hydraulic methods being developed within CASL.

Flow Regime Maps

The flow regime map in COBRA-TF is based solely on void fraction. This is in contrast to most flow regime maps incorporated into reactor systems codes which include both void fraction and mass flux. For the simulation of nominal PWR conditions, void fractions are generally less than about 25%, which for the COBRA-TF map corresponds to small bubbles. Under these conditions, COBRA-TF will draw from the correct correlations. Consideration should be given to upgrading the flow regime map if simulations outside of this parameter range are expected.

Wall Drag

Prior to critical heat flux, the pressure drop due to wall drag is completely allocated to the liquid phase according to

$$\left.\frac{\partial P}{\partial z}\right|_{frict} = \frac{f_w\left(\rho_l v_l\right)^2}{2D_e\rho_l}$$

There is no additional wall drag as a result of the vapor phase being generated at the wall, and no partitioning of the total pressure drop between phases. This approach is again more directly applicable to annular flow and unlikely to provide the correct two phase pressure drop in other flow regimes. RELAP-5 and TRACE are two reactor systems codes based on the six equation model that compute the two phase drop through the use of more advanced two-phase multipliers and wall drag partitioning schemes. TRACE [5] computes the two phase pressure drop in a manner identical to that found in CTF, but only in the case of annular flow. For example, in the bubbly flow regime, the liquid phase component of the pressure drop is formulated as

$$\left.\frac{\partial P}{\partial z}\right|_{fricl,l} = \frac{f_w \left(G_l\right)^2}{2D_e \rho_l} \Phi_l^2$$

where

$$\Phi_l^2 = \frac{1}{\alpha_l^{1.72}}$$

TRACE then partitions the wall drag such that for all flow regimes prior to CHF (bubbly, annular/mist, etc.) all of the wall drag is partitioned to the liquid phase. RELAP-5 [6] computes a two phase multiplier based on the Lockhart-Martinelli parameter

$$\Phi_l^2 = 1 + \frac{C}{\chi} + \frac{1}{\chi^2}$$

and then partitions the pressure drop between phases based on a method derived from a quasi-steady form of the momentum equation.

Fuel Rod Temperatures and Heat Generation Rates

COBRA-TF has the ability to perform limited three dimensional heat conduction in fuel rods. The azimuthal direction is limited to four nodes, one per quadrant. This coarse nodalization is consistent with the subchannel representation of fluid temperature, where only the quadrant average temperatures are available. Heat generation rates in COBRA-TF can only be specified radially and axially within a rod, so any azimuthal variation in fuel temperature will be due solely to the differences in the subchannel fluid temperatures and heat transfer coefficients.

Steady-State Capabilities

COBRA-TF is a purely transient code. Steady state conditions are obtained by running the code until a user specified convergence criteria is met. This approach may create issues if the impact of small perturbations on the solution is to be evaluated.

References


1) F. S. Castellana and J. E. Casterline, "Subchannel flow and enthalpy distributions at the exit of a typical nuclear fuel core geometry," *Nuclear Engineering and Design,* vol. 22, no. 1, pp. 3-18, 1972.

2) Subcooled Boiling Data From Rod Bundles, EPRI, Palo Alto, CA; 2002. 1003383.

3) Robert K. Salks and Maria N. Avramova, "CTF Theory Manual", Department of Mechanical and Nuclear Engineering, The Pennsylvania State University, June 21, 2012

4) D. Basile, M. Beghi, R. Chierici, E. Salina and E. Brega, "COBRA-EN, An upgraded version of the COBRA-3C/MIT code for thermal-hydraulic transient analysis of light water reactor fuel assemblies and cores," Radiation Safety Information Computational Center, Oak Ridge National Lab, 1999.

5) TRACE V5.0 Theory Manual. "Field Equations, Solution Methods and Physical Models." US NRC, Washington DC.

6) RELAP-5 3D Code Manual. "Volume 1: Code Structure, System Models and Solution Methods." Idaho National Engineering and Environmental Laboratory, Idaho Falls.